Available online at www.sciencedirect.com
SCIENCE DIRECT
Trans. Nonferrous Met. Soc. China 18(2008) 1164−1171
Transactions of Nonferrous Metals Society of China
www.csu.edu.cn/ysxb/

Quasicontinuum simulation of indentation on FCC metals

WANG Hua-tao(王华滔), QIN Zhao-dong(秦昭栋), NI Yu-shan(倪玉山), ZHANG Wen(张 文)
Department of Mechanics and Engineering Science, Fudan University, Shanghai 200433, China

Received 22 January 2008; accepted 30 May 2008

Abstract: Quasicontinuum simulations were performed to study the processes of incipient plastic deformation on three FCC metals (Ag, Ni and Pd) under the action of a rigid indenter. Four widths (9.3, 18.6, 27.9 and 37.2 Å) of the indenters were modelled for each metal specimen. A series of load—displacement responses and the strain energy versus displacement responses of the indenter were presented. It is shown that the abrupt drop of the load in the load—displacement response is triggered by the nucleation of dislocations in the metals. The critical load of each metal specimen increases with the increase of the indenter width, while the hardness of the metal specimen decreases as the indenter width increases. Furthermore, the microscopic mechanism of deformation in the films was analyzed. Two dislocations are nucleated respectively beneath the right and left sides of the indenter. Each dislocation successively decomposes into two Shockley partial dislocations after the first nucleation process. The distances between the two partial dislocations are equal for both sides of the indenter, which are in agreement with the theoretical values.

Key words: indentation; quasicontinuum method; dislocation; nucleation

1 Introduction

Nano-scale contact of material surfaces provides an opportunity to explore the elastic limit and incipient plasticity in crystals. One popular and relatively simple experimental technique in this domain is nanoindentation [1], which is the penetration of a surface to nanometre depth using an indenting device. It is proved to be a useful tool for studying the onset of plastic deformation in crystals[2]. Nanoindentation of FCC metals causes a load — displacement sharp decline response that is separated into regions of elastic deformation and discrete displacement bursts[3−5]. Interpretation of the phenomenon is further complicated by the fact that the response can highly be dependent on the indenter geometry and its orientation[6]. It can also be strongly influenced by additional factors such as surface effects[7], substrate effects[8], grain effects[9] and pre-existing defects[10].

Interpretation of the sharp decline response may be facilitated by a clear understanding of the processes taking place during the numerical simulations. In recent years, there have been a number of simulations of nanoindentation, which led to great insight into the microscopic phenomena of nanoindentation. GOULDSTONE et al[11] have used the Bragg–Nye bubble raft model to simulate the indentation in {111} plane of FCC crystal. It demonstrated that nanoindentation of a two-dimensional crystal may lead to homogeneous nucleation of dislocations within the crystal. Quasicontinuum(QC) simulations by TADMOR et al[12] via the QC method revealed the process of nanoindentation-induced dislocation nucleation near the surface in single crystal aluminium. However, a quantitative analysis of the partial dislocations decomposed from the dislocation nucleation of nanoindentation is still lacking. SANSOZ et al[13] and WARNER et al[14] have extended the QC method to study the properties in nanoindentation of nanocrystalline metals.

In this work, QC method was employed to analyze the processes of incipient plastic deformation on three FCC metals (Ag, Ni and Pd) under the action of a rigid indenter. To investigate the size effect of the indenter, each metal specimen was modelled with the four widths D (9.3, 18.6, 27.9 and 37.2 Å) of indenters. A series of load—displacement responses and the strain energy versus displacement responses of the indenters were presented. For a deep understanding of the nature in the

Foundation item: Project(10576010) supported by the National Natural Science Foundation of China and NSAF Foundation of China
Corresponding author: NI Yu-shan; Tel: +86-21-55665173; E-mail: niyushan@fudan.edu.cn

nucleation of the dislocations, the microscopic mechanisms of dislocation deformation were investigated.

2 QC modeling

2.1 Governing equations

The QC method[15] is a mixed continuum and atomistic approach for simulating the mechanical response of the crystal materials. The finite element method serves as the numerical engine for determining the energy minimizing displacement fields, while the atomistic analysis is used to determine the energy of a given configuration. The very important point of atomistic method is the determination of the total potential energy of a system as a function of the degrees of freedom(DOF). The static equilibrium at 0 ℃ is followed by minimizing the total energy or finding the zero-force positions for every DOF. The force on a DOF is the derivative of the total energy with respect to the DOF coordinate. The total atomic energy has the following form:

$$E^{\mathrm{a}} = \sum_i E_i(u) \tag{1}$$

where $E_i(u)$ is the energy of the ith atom, u is the displacement of the ith atom. The total atomic energy is written as a sum over the energy of each atom.

The embedded-atom method(EAM)[16] is used to calculate the energy of a single atom:

$$E_i = F_i\left(\sum_{j\neq i}\rho_j(r_{ij})\right) + \frac{1}{2}\sum_{j\neq i}V_{ij}(r_{ij}) \tag{2}$$

where F_i is an electron-density dependent on embedding energy; V_{ij} is a pair potential between atom i and its neighbor j; r_{ij} is the inter-atomic distance; ρ_j is the density contributions from each of the neighbors.

The QC method is a multi-scale technique based on the idea of representative atoms and finite element interpolation. Instead of treating all atoms making up the system, a small relevant subset of atoms is selected to represent the whole energetic of the system. Based on their kinematical environment, the energies of individual "representative atoms" are computed either in nonlocal fashion in correspondence with straightforward atomistic methodology or within a local approximation as befitting a continuum model. The representation is of varying density with more atoms sampled in highly deformed regions (such as near defect cores) and correspondingly fewer in the less deformed regions further away, and is adaptively updated as the deformation evolves:

$$u = \sum_{\alpha=1}^{N_{\mathrm{rep}}} S_\alpha u_\alpha \tag{3}$$

where S_α is a interpolation function associated with the repatom α; u_α is the displacement of the repatom and N_{rep} is the number of the repatoms. It is shown that the number of the repatoms is much less than that of the total atoms in the system of $N_{\mathrm{rep}} \ll N$.

The interface atoms are the nodes of the atomistic domain as well as the finite element nodes of the continuum domain. To avoid the overlap computing of the energy of the interface atoms, we can use different weighting conditions on the atoms between the continuum regions and the atomistic ones. Thus, the repatoms are divided into local repatoms and nonlocal repatoms ($N_{\mathrm{loc}}+N_{\mathrm{nl}}=N_{\mathrm{rep}}$). The total energy expression in the QC model is then approximated as

$$E^{\mathrm{tot}} = \sum_{\mu=1}^{N_{\mathrm{loc}}} n_\mu E_\mu(u) + \sum_{\alpha=1}^{N_{\mathrm{nl}}} n_\alpha E_\alpha(u) \tag{4}$$

where n_μ and n_α are the weight function of the local repatoms and the nonlocal ones, respectively; E_μ is the energy of the local elements; E_α is the energy of the nonlocal repatoms; n_α is the exact unity for all the elements that are not connected to the interface. For the elements connected to the interface, the weight functions depend on the shape of the elements, but always satisfy $0<n_\mu<1$ and $0<n_\alpha<1$.

2.2 Simulation procedures

Quasicontinuum simulations are performed to study the processes of the initial plastic deformation under the action of a rigid indenter on three FCC metals (Ag, Ni and Pd). Four widths (9.3, 18.6, 27.9 and 37.2 Å) of the indenters are modelled for each metal specimen. The Ercolessi-Adams EAM potential was adopted in the micro-scale. The size of the simulated thin film is 2 000 Å in x[111] direction, 1 000 Å in $y[\bar{1}10]$ direction, and 8.064 Å (a distance of two planes) in $z[\bar{1}\,\bar{1}2]$ direction, as shown in Fig.1.

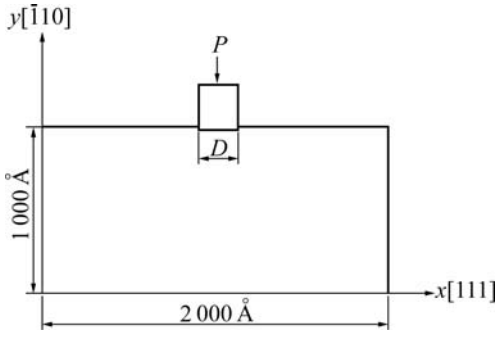

Fig.1 Geometric drawing of indentation model

The system investigated here consists of 1.3 million atoms. By using the QC method, only 4 000 atoms are chosen as repatoms treated explicitly (12 000 degrees of freedom), and the computational intensity is greatly reduced. The region to be represented as either atomistic

or continuum is determined by evaluating the magnitude of evolving local deformations, which can be characterized by

$$\max_{a,b,k}\left|\lambda_k^a-\lambda_k^b\right|<\varepsilon \tag{5}$$

where a and b run over all elements that are within two radius distance of the representative atom; λ_k^a and λ_k^b are the kth eigenvalues of the right stretch tensor obtained from the deformation gradient in the element a and b; ε is an empirically selected constant, which is chosen to be 0.1 in this work.

Periodic boundary condition is adopted in z-direction. The maximum displacement of the indenter contrasted to the thickness of the film is still very small, thus the far-field boundary conditions will not affect the result of the computation. For FCC metals, the (111) crystal plane is the close-packed plane of atoms, in which the dislocation can be nucleated advantageously. Since (111) plane is perpendicular to the [111] direction, we choose the preferential (x[111], y[$\bar{1}$10], z[$\bar{1}\,\bar{1}$2]) orientation during the simulations to investigate the nucleation of the dislocations easily. As for another crystal orientation, there will be another mechanism of the deformation. For example, if the specimen crystallography is set to be (x[$\bar{1}\,\bar{1}$2], y[111] and z[$\bar{1}$10]), the microcosmic deformation is led by the deformation twinning rather than the nucleation of the dislocation. The effect of the crystal orientation in nanoindentation simulation was studied in Refs.[6,12]. For each film, the four widths (9.3, 18.6, 27.9 and 37.2 Å) of indenters were chosen. The simulation was conducted by controlling the displacement of the indenter, and the indenter dropped about 0.2 Å to the inferior of the films at each step. We performed 40 steps in this modeling until the depth of the indentation reaches 8 Å and the energy minimization was executed in the end of each step.

3 Results and discussion

3.1 Load—displacement response and strain energy variations for various metals

The force on every atom at each step is the partial derivative of the function E^a with respect to the coordinate of the atom:

$$f_i=-\frac{\partial E^a\{r_1\cdots r_n\}}{\partial r_i} \tag{6}$$

The total force under the indenter is the sum of the force on each atom. The load—displacement curves for the films of various metals are shown in Fig.2(a), Fig.3(a) and Fig.4(a), respectively. The energy variations for the

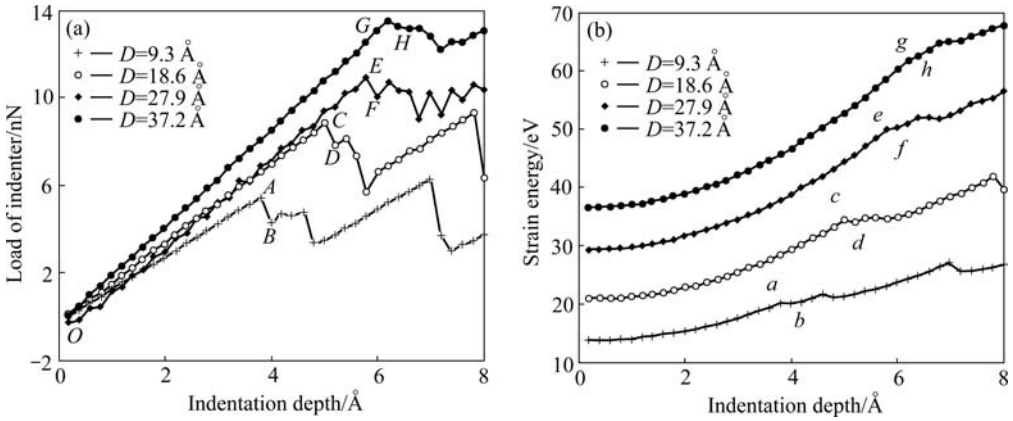

Fig.2 Load (a) and strain energy (b) vs displacement response for Ag films

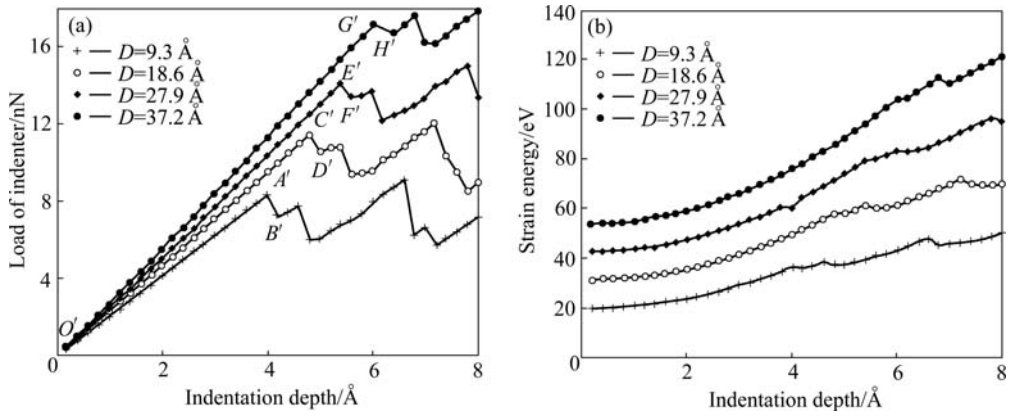

Fig.3 Load (a) and strain energy (b) vs displacement response for Ni films

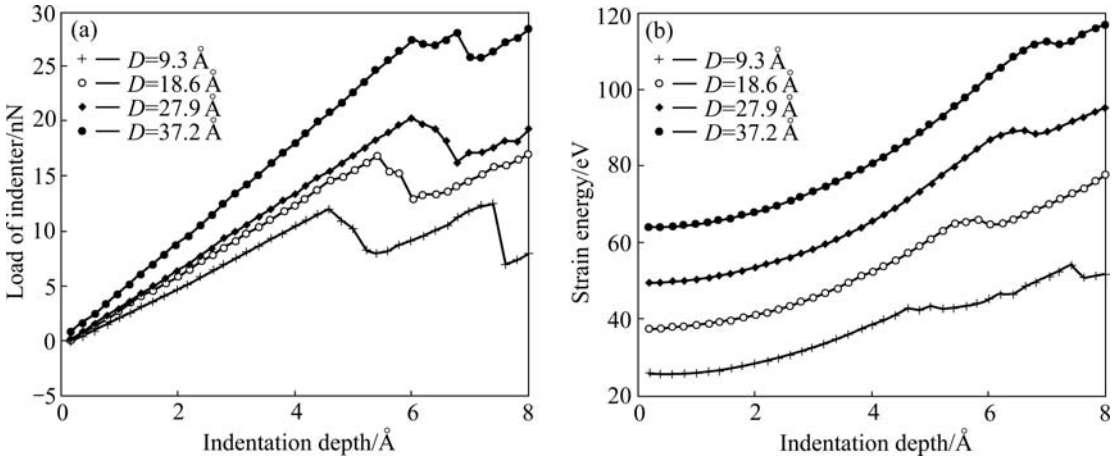

Fig.4 Load (a) and strain energy (b) vs displacement response for Pd films

films are shown in Fig.2(b), Fig.3(b) and Fig.4(b), respectively.

At the initial stages of load (*OA*, *OC*, *OE* and *OG* in Fig.2(a)) for Ag film under various indenter widths, the load—displacement curves are linear, which indicates that each film deforms elastically. The load of indenter reaches different ultimate values at points *A*, *C*, *E* and *G* in Fig.2(a), in which corresponding displacements of the indenters are 3.8, 5, 5.8 and 6.2 Å. With increasing loading, all of the load—displacement curves encounter one abrupt drop (*AB*, *CD*, *EF* and *GH* in Fig.2(a)). During this stage, the film is suffered from a plastic deformation, and the dislocation is triggered to nucleate beneath the indenter, which is in good agreement with Ref.[19]. The slope of each line in Fig.2(a) becomes larger and larger with the increase of the indenter width at the initial stage, and the critical load of the plastic deformation is strengthened as well. It is considered to be a size effect of the width of the indenters.

The energy of each width at the initial stage increases with the increase of the indentation depths for Ag crystal of various indenter widths (9.3, 18.6, 27.9 and 37.2 Å), as shown in Fig.2(b). The energy increases slowly (*ab*, *cd*, *ef* and *gh*) in the energy variations. After this step, the energy will continue to increase as before, which shows that the material is hardened. The deformation processes with the indenter widths (18.6, 27.9 and 37.2 Å) are the same as those of 9.3 Å, but the nucleated time becomes later and later with the increase of the indenter width. The energy variation at each time in Fig.2(b) is corresponded to the load variation in the load—displacement response in Fig.2(a).

Fig.3(a) for Ni film is the same as Fig.2(a) for Ag film at the initial stage (*O′A′*, *O′C′*, *O′E′* and *O′G′* in Fig.3(a)). Each film deforms elastically until a dislocation nucleation event occurs. The load of indenters reaches the ultimate value at points *A′*, *C′*, *E′* and *G′*, and the corresponding displacements of the indenters are 4.2, 5, 5.6 and 6.2 Å. All of the load—displacement curves meet one abrupt drop (*A′B′*, *C′D′*, *E′F′* and *G′H′*) with increasing the load in Fig.3(a). The slope of each line in Fig.3(a) increases slightly with the increase of the indenter width, and the critical load of the elastic deformation increases as well.

The energy variation at each time in Fig.3(b) is corresponded to the load variation in the load—displacement response in Fig.3(a).

Similarly, at the initial stage in Fig.4(a) for Pd, each film deforms elastically until a dislocation nucleation event occurs. The load of indenters reaches the ultimate value, and the corresponding displacements of the indenters are 4.8, 5.6, 6.2 and 6.6 Å. Following the process of the load, all of the load—displacement curves in Fig.4(a) show one abrupt drop. The deformation becomes non-linear, and the dislocations are nucleated. The slope of each line increases slightly with the increase of the indenter width and the critical load of the elastic deformation increases as well.

The energy variation at each time in Fig.4(b) is corresponded to the load variation in the load—displacement response in Fig.4(a).

3.2 Hardness of three films under various indenter widths

The hardness of each film can be calculated by

$$H=\frac{\sigma}{S} \tag{7}$$

where σ is the ultimate value of the load at the initial elastic stage; S is the contact area between the indenter and the film. The changes of the hardness for the films under various indenter widths are listed in Table 1. As shown more clearly in Table 1, the hardness for each metal specimen decreases with the increase of the indenter width, which is in good agreement with Refs.[17−19].

Table 1 Hardness of three films under various indenter widths (GPa)

Film	D=9.3 Å	D=18.6 Å	D=27.9 Å	D=37.2 Å
Ag	11.68	9.50	7.88	7.22
Ni	33.30	22.84	18.67	17.08
Pd	26.78	18.96	15.24	12.53

3.3 Mechanisms of dislocation nucleation

Dislocations are nucleated just beneath both the right and the left side of the indenter. In nucleation, the dislocation dissociates into two partial dislocations: one partial dislocation glides into the crystal and the other runs to the surface.

Specifically, the left dislocation dissociates into two partial dislocations according to the following principle [20]:

$$\frac{1}{2}[\bar{1}10] \rightarrow \frac{1}{6}[\bar{1}2\bar{1}]+\frac{1}{6}[\bar{2}11] \tag{8}$$

and the right dislocation dissociates into two partial dislocations:

$$\frac{1}{2}[1\bar{1}0] \rightarrow \frac{1}{6}[1\bar{2}1]+\frac{1}{6}[2\bar{1}\bar{1}] \tag{9}$$

After the decomposition of the dislocation, the two partial dislocations form a stacking fault between them, as shown in Fig.5.

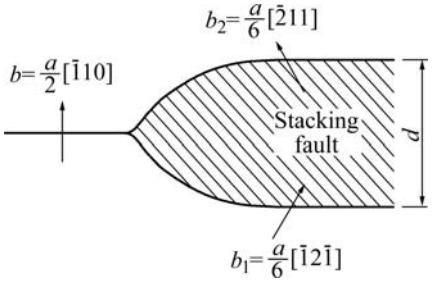

Fig.5 Decomposed process of dislocation under left side of indenter[20]

Corresponding to the load—displacement response of Fig.2(a), Fig.3(a) and Fig.4(a), respectively, we plot the nucleation of the dislocations in the UZ deformation (Figs.6, 7 and 8), in which the distributions of the

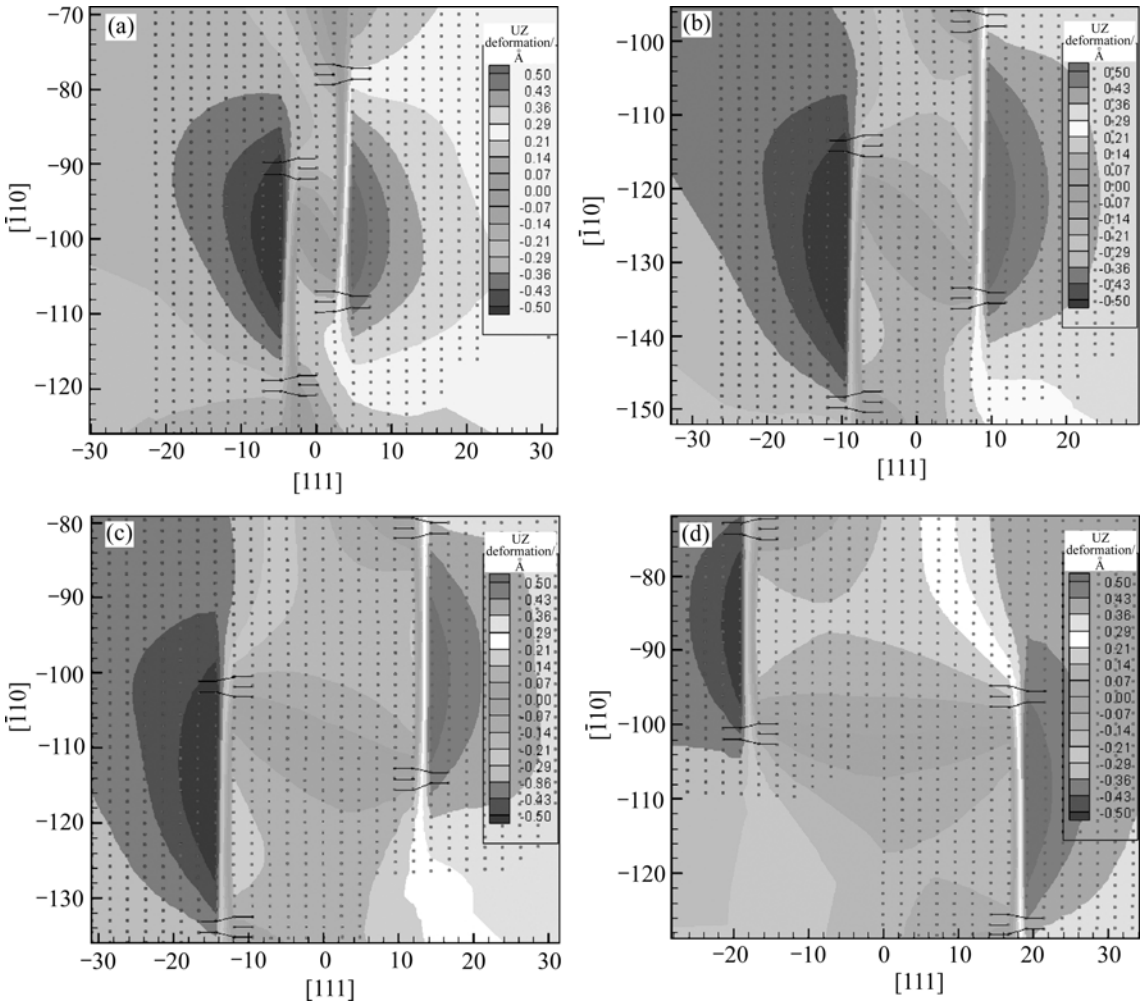

Fig.6 UZ contour plots of Ag film under indenter width of 9.3 Å at 20th load step (a), indenter width of 18.6 Å at 26th load step (b), indenter width of 27.9Å at 30th load step (c) and indenter width of 37.2 Å at 32nd load step (d)

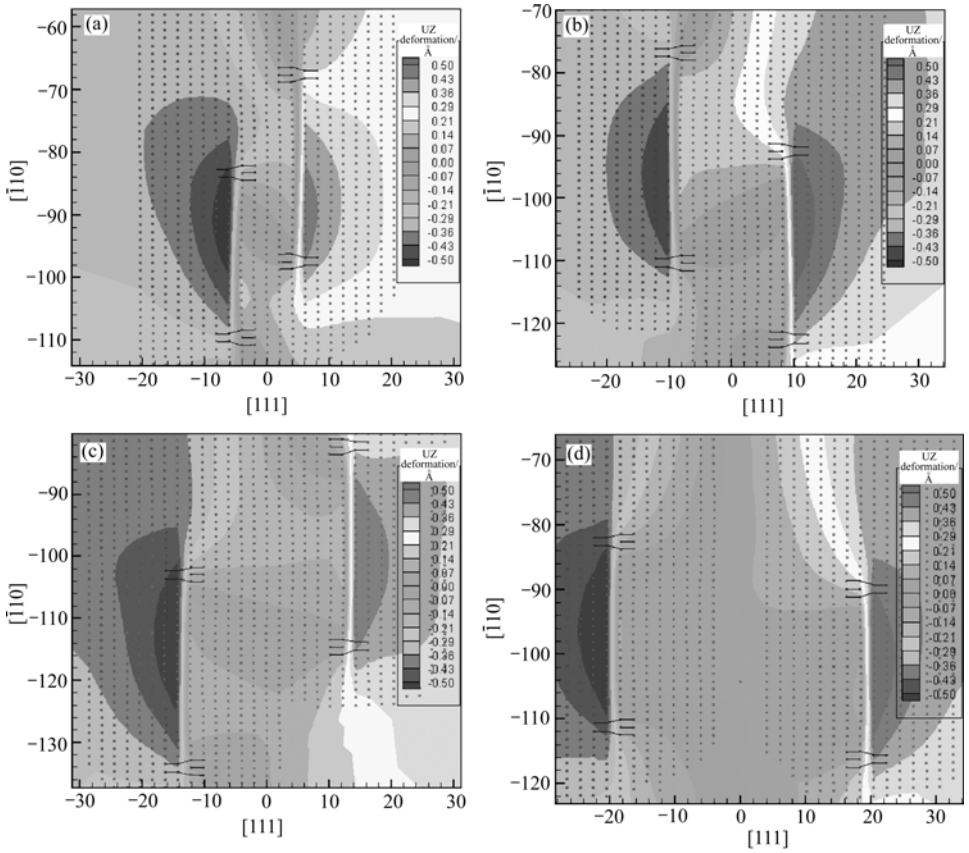

Fig.7 UZ contour plots of Ni film under indenter width of 9.3 Å at 22nd load step (a), indenter width of 18.6 Å at 26th load step (b), indenter width of 27.9 Å at 29th load step (c) and indenter width of 37.2 Å at 32nd load step (d)

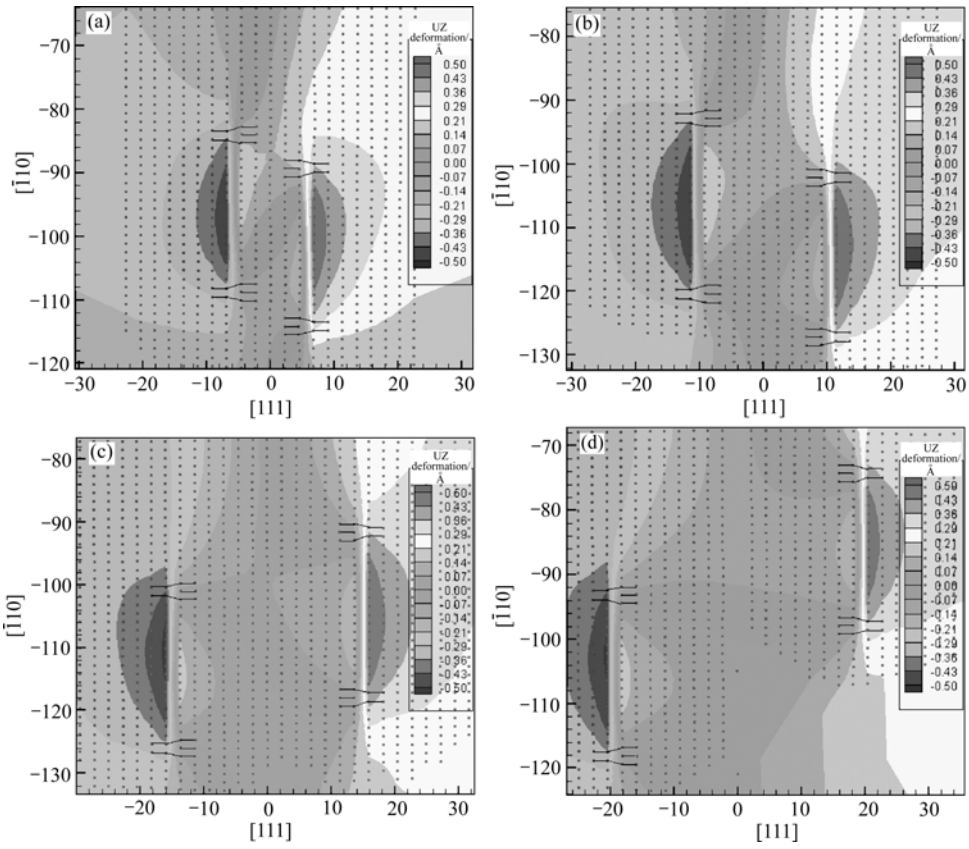

Fig.8 UZ contour plots of Pd film under indenter width of 9.3 Å at 25th load step (a), indenter width of 18.6 Å at 29th load step (b), indenter width of 27.9 Å at 32nd load step (c) and indenter width of 37.2 Å at 34th load step (d)

repatoms and the locality of the dislocation are marked, respectively. Because the perfect dislocation is nucleated in the form of two partial dislocations, it can not be found in the atomic plots.

From Fig.6 to Fig.8, it is found that the distance between two Shockley partials on the left side and the right side of the indenter are the same for each metal specimen. The distance between the two Shockley partials on both sides of the indenter is plotted in Fig.9(a) and Fig.9(b), respectively.

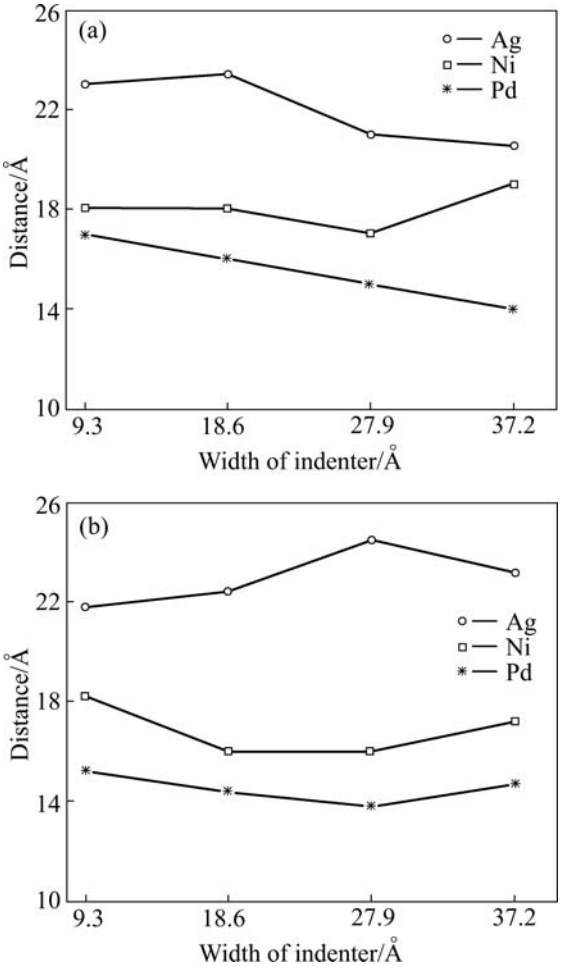

Fig.9 Distance between two Shockley partials on left side of indenter (a) and right side of indenter (b)

The theoretical width of the partial dislocations can be calculated by the balance relations of the force and the stacking fault energy between the two partial dislocations as[20]

$$d_0 = \frac{\mu a^2 (2+\nu)}{24\pi(1-\nu)\gamma} \tag{10}$$

where d_0 is the width of the partial dislocations; μ is the $<11\bar{2}>\{111\}$ shear module; ν is the Poisson ratio; a is the lattice constant; and γ is the default energy. Both theoretical and computational widths of the partial dislocations are listed in Table 2.

It can be seen from Table 2 that the width of the partial dislocations beneath each side of the indenter in this simulation is in agreement with the theoretical analysis approximately. The error between them (especially Ag) might be due to the sources of the microscopic parameters or the EAM potential used in the calculation.

Table 2 Comparison between simulated and theoretical width of partial dislocations

Metal	μ/MPa	ν	a/Å
Ag[20]	27.8	0.434	4.09
Ni[20]	80.7	0.351	3.52
Pd[12]	53.8	0.373	3.89
Metal	γ/(mJ·m^{-2})	$d_{0,\,simu}$/Å	$d_{0,\,theore}$/Å
Ag[20]	47	31.5	56.5
Ni[20]	140	29.9	34.3
Pd[12]	180	25.1	22.7

4 Conclusions

1) At the initial stage of the indentation, each metal specimen deforms elastically. Subsequently, the load—displacement responses of all specimens are encountered an abrupt drop, which demonstrates that the abrupt drop of the load is triggered by the nucleation of dislocations in the metals.

2) The critical load of each metal specimen increases with the increase of the indenter width, while the hardness of the metal specimen decreases as the indenter width increases.

3) Two dislocations are nucleated respectively beneath the right and left sides of the indenter. Each dislocation successively decomposes into two Shockley partial dislocations after the first nucleation process. The distance between the two partial dislocations is equal for both sides of the indenter.

References

[1] NIX W D. Mechanical properties of thin films [J]. Metallurgical Transactions A, 1989, 20A: 2217−2245.

[2] SUTTON A P, PETHICA J B. Inelastic flow processes in nanometer volumes of solids [J]. Journal of Physics: Condensed Matter, 1990, 2: 5317−5326.

[3] SURESH S, NIEH T G, CHOI B W. Nano-indentation of copper thin films on silicon substrates [J]. Scripta Materialia, 1999, 41: 951−957.

[4] GOULDSTONE A, KOH H J, ZENG K Y. Discrete and continuous deformation during nanoindentation of thin films [J]. Acta Materialia, 2000, 48: 2277−2296.

[5] GERBERICH W W, NELSON J C, LILLEODDEN E T, ANDERSON P, WYROBEK J T. Indentation induced dislocation

nucleation: The initial yield point [J]. Acta Materialia, 1996, 44: 3585−3598.

[6] IGLESIAS R A, LEIVA E P. Two-grain nanoindentation using the quasicontinuum method: Two dimensional model approach [J]. Acta Materialia, 2006, 54: 2655−2664.

[7] GANE N, BOWDEN F P. Microdeformation of solids [J]. Journal of Applied Physics, 1968, 39: 1432−1435.

[8] ZHAO Lei, LIAN Jian-she. Effect of substrate temperature on structural properties and photocatalytic activity of TiO_2 thin films [J]. Trans Nonferrous Met Soc China, 2007, 17(3): 772−776.

[9] TANGYUNYONG P, THOMAS R C, HOUSTON J E, MICHALSKE T A, CROOKS R M, HOWARD A J. Nanometer-scale mechanics of gold films [J]. Physical Review Letter, 1993, 71: 3319−3322.

[10] PHARR G M, OLIVER W C. Nanoindentation of silver—relations between hardness and dislocation structure [J]. Journal of Materials Research, 1989, 4: 94−101.

[11] GOULDSTONE A, VLIET K J, SURESH S. Simulation of defect nucleation in a crystal [J]. Nature, 2001, 411: 656.

[12] TADMOR E B, ORTIZ M, PHILLIPS R. Quasi-continuum analysis of defects in solids [J]. Journal of Materials Research, 1999, 14: 2234−2242.

[13] SANSOZ F, DUPONT V. Deformation of nanocrystalline metals under nanoscale [J]. Applied Physics Letters, 2006, 89: 111901−1−111901−3.

[14] WARNER D H, SANSOZ F, MOLINARI J F. Atomistic based continuum investigation of plastic deformation in nanocrystalline copper [J]. International Journal of Plasticity, 2006, 22(4): 754−774.

[15] SHENOY V B, MILLER R, TADMOR E B, PHILLIPS R, ORTIZ M. Quasicontinuum models of interracial structure and deformation [J]. Physical Review Letters, 1998, 80(4): 742−745.

[16] ERCOLESSI F, ADAMS J B. Interatomic potentials from first-principles calculations: The force-matching method [J]. European Physical Letters, 1994, 26: 583−592.

[17] SHENOY V, PHILLIPS R, TADMOR E B. Nucleation of dislocations beneath a plane strain indenter [J]. Journal of the Mechanics and Physics of Solids, 2000, 48: 649−673.

[18] POOLE W J, ASHBY M F, FLECK N A. Micro-hardness of annealed and work-hardened copper polycrystals [J]. Scripta Materialia, 1996, 34: 559−564.

[19] MANIKA I, MANIKS J. Size effects in micro- and nanoscale indentation [J]. Acta Materialia, 2006, 54(8): 2049−2056.

[20] GEROLD V. Structure of solids [M]. New York: Cambridge, 1993: 393.

(Edited by LI Xiang-qun)